AGU PUBLICATIONS

JGR

Journal of Geophysical Research: Solid Earth

RESEARCH ARTICLE

10.1002/2016JB013767

Key Points:
- Temperature has more greatly influence on electrical conductivity of epidote than pressure
- Dehydration reaction was investigated around 1073 K by the variation of electrical conductivity
- Aqueous fluids from epidote dehydration can explain the highly conductive anomalies in the mantle wedge below 70 km, especially in the hot subduction zones

Correspondence to:
L. Dai,
dailidong@vip.gyig.ac.cn

Citation:
Hu, H., L. Dai, H. Li, K. Hui, and W. Sun (2017), Influence of dehydration on the electrical conductivity of epidote and implications for high-conductivity anomalies in subduction zones, *J. Geophys. Res. Solid Earth*, *122*, 2751–2762, doi:10.1002/2016JB013767.

Received 17 NOV 2016
Accepted 1 APR 2017
Accepted article online 5 APR 2017
Published online 22 APR 2017

Influence of dehydration on the electrical conductivity of epidote and implications for high-conductivity anomalies in subduction zones

Haiying Hu[1], Lidong Dai[1], Heping Li[1], Keshi Hui[1,2], and Wenqing Sun[1,2]

[1]Key Laboratory for High-temperature and High-pressure Study of the Earth's Interior, Institute of Geochemistry, Chinese Academy of Sciences, Guiyang, Guizhou, China, [2]University of Chinese Academy of Sciences, Beijing, China

Abstract The anomalously high electrical conductivities (~0.1 to 1 S/m) in deep mantle wedge regions extensively detected by magnetotelluric studies are often associated with the presence of fluids released from the progressive dehydration of subducting slabs. Epidote minerals are the Ca-Al-rich hydrous silicates with huge stability fields exceeding those of amphibole (>70–80 km) in subducting oceanic crust, and they may therefore be transported to greater depth than amphibole and release water to the mantle wedge. In this study, the electrical conductivities of epidote were measured at 0.5–1.5 GPa and 573–1273 K by using a Solartron-1260 Impedance/Gain-Phase Analyzer in a YJ-3000t multianvil pressure within the frequency range of 0.1–10^6 Hz. The results demonstrate that the influence of pressure on electrical conductivity of epidote is relatively small compared to that of temperature. The dehydration reaction of epidote is observed through the variation of electrical conductivity around 1073 K, and electrical conductivity reaches up to ~1 S/m at 1273 K, which can be attributed to aqueous fluid released from epidote dehydration. After sample dehydration, electrical conductivity noticeably decreases by as much as nearly a log unit compared with that before dehydration, presumably due to a combination of the presence of coexisting mineral phases and aqueous fluid derived from the residual epidote. Taking into account the petrological and geothermal structures of subduction zones, it is suggested that the aqueous fluid produced by epidote dehydration could be responsible for the anomalously high conductivities in deep mantle wedges at depths of 70–120 km, particularly in hot subduction zones.

1. Introduction

A large number of electromagnetic and seismic results from various subduction zones indicate the presence of anomalies of electrical conductivity (EC) and seismic wave attenuation in the mantle wedge and fore-arc regions. In these regions, electrical conductivity is characterized by the high value of ~0.1–1 S/m [*Soyer and Unsworth*, 2006; *Chen and Clayton*, 2009; *Pozgay et al.*, 2009; *Worzewski et al.*, 2011; *Evans et al.*, 2014; *Pommier*, 2014]. By combining petrological studies [*Liu et al.*, 1996; *Ono*, 1998; *Schmidt and Poli*, 1998] with experimentally conductivity measurements [*Guo et al.*, 2011; *Ni et al.*, 2011; *Wang et al.*, 2012; *Manthilake et al.*, 2015, 2016], the high conductivity anomalies in these regions are commonly explained by the presence of partial melt or free fluids released from dehydration of hydrous minerals (e.g., amphibole, chlorite, lawsonite, zoisite/epidote, chloritoid, and talc) in the subducting slab. In the setting of young and hot subduction zones, partial melting in the mantle wedge, caused by ascending fluids released from the subducting oceanic lithosphere or escaped along fracture zones to the upper mantle, is often at depths shallower than 70 km [*Liu et al.*, 1996]. However, for the mature and cold subduction zone with low thermal gradient, hydrous minerals are stable to greater depth along the subducting slab and a large amount of water released from the dehydration of these minerals takes place at depths even greater than 100 km [*Poli and Schmidt*, 1995], also causing partial melting of the deep mantle wedge overlying the subduction slab. Consequently, the interpretations for the highly conductivity anomalies in the deep mantle wedge as a result of the release of deep fluids or partial melting are still in debate. However, the laboratory-based EC measurements on hydrous minerals in subduction slabs can provide an independent and important constraint on the interpretation of the anomalous high conductivity observed in field magnetotelluric (MT) results, because electrical conductivity is strongly dependent on the variation of water content in sample, partial melting, and temperature.

Extensive laboratory work has sought to measure the electrical conductivity of the major hydrous phases in subduction zones such as serpentinites and talc [*Guo et al.*, 2011; *Reynard et al.*, 2011; *Wang and Karato*, 2013],

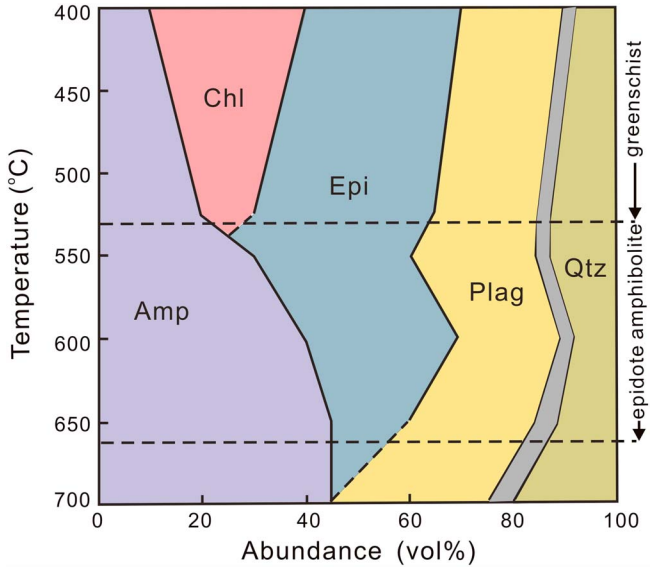

Figure 1. Temperature-abundance diagram for hydrated MORB composition. Data from *Apted and Liou* [1983]. Abbreviations: Amp, amphibole; Chl, chlorite; Epi, epidote; Plag, plagioclase; Qtz, quartz.

amphibole [*Wang et al.*, 2012], lawsonite [*Manthilake et al.*, 2015], phlogopite [*Li et al.*, 2016], and chlorite [*Manthilake et al.*, 2016], but large differences are evident in the results of these experiments, and in some cases, the laboratory measurement results are inconsistent with field MT observations. Additionally, the mechanism of enhanced electrical conductivity of hydrous minerals during dehydration temperature regime is still controversial. For instance, the enhanced conductivity of amphibole and talc at temperatures exceeding the stability field of samples is considered to be due to the oxidation of iron rather than aqueous fluid released during dehydration [*Wang et al.*, 2012; *Wang and Karato*, 2013]. The electrical conductivity results of phlogopite also showed that the conductivity is not caused by water, but probably F and K [*Li et al.*, 2016]. Recent experimental study on electrical conductivity of chlorite demonstrated that aqueous fluid alone cannot explain the anomalously high conductivity in the mantle wedge, but an interconnected network of chemically impure magnetite produced during the dehydration of chlorite does [*Manthilake et al.*, 2016]. In addition, molecular dynamic simulation results reveal that the presence of low-salinity (0.5 wt %) NaCl-H_2O fluid can account for the anomalous high-conductivity zones at a relative shallow depths above the subducting oceanic crust [*Sakuma and Ichiki*, 2016]. Consequently, it remains unknown whether the presence of other conductive materials other than aqueous fluid is required to explain the high EC in the subduction zone.

The epidote group is a complex family of rock-forming silicate minerals with the chemical formula $Ca_2Al_{3-x}Fe_xSi_3O_{13}H$ ($0 < x < 1.0$) [*Franz and Selyerstone*, 1992; *Kvick et al.*, 1988; *Grodzicki et al.*, 2001]. Monoclinic members up to 0.5 Fe per formula unit (pfu) are commonly called clinozoisite, and those with more than 0.5 Fe pfu are named epidote. Epidote is unequivocally a reaction product when the oceanic crust passes through the greenschist to blueschist facies metamorphism, simultaneously a progressive increase of epidote abundance with pressure, and its high abundance reaches 30–35 vol % occurring in epidote-blueschist facies as shown in Figure 1 [*Apted and Liou*, 1983; *Poli and Schmidt*, 2004]. Additionally, the huge stability field of epidotes means that they often have been considered to be an significant water reservoir in subducting oceanic crust at depths exceeding the stability of amphibole (>70–80 km), even at higher geothermal gradients, which implies that epidote/zoisite could contribute to fluid flux to the mantle wedge at depths of 100–120 km [*Poli and Schmidt*, 1995, 1998; *Liu et al.*, 1996]. Hence, the aqueous fluids released by epidote dehydration in the context of subduction may be responsible for the anomalously high conductivity in the deep mantle wedge. However, no study has been devoted to the electrical conductivity of epidote under the conditions prevailing in subduction zones and its possible contribution to the anomalously high conductivity regions in the deep mantle wedge.

2. Experimental Procedures

The starting materials were gem-quality, short prismatic single crystals of green epidote from Handan in Hebei province, China. The chemical compositions of samples were determined with an EPMA-1600 electron probe operating at an accelerating voltage of 25 kV and a beam current of 10 nA, and the results are shown in Table 1. The crystals are chemically homogeneous determined by multipoint electron microprobe analyses. Cylindrical cores with 6.0 mm in diameter and 3.0–6.0 mm in length were prepared by cutting and polishing natural crystals along the direction of *b* axis. The samples were then successively cleaned by using acetone

Table 1. The Chemical Composition of Sample Before Electrical Conductivity Measurement (wt %)[a]

Sample	SiO_2	Al_2O_3	CaO	MgO	TiO_2	MnO	Fe_2O_3	Na_2O	Total
Epi	39.27	22.18	23.49	0.03	0.03	0.04	12.25	0.03	97.32

[a]All Fe in epidote as Fe^{3+}.

and ethanol in an ultrasonic cleaner and later stored in a muffle furnace at 423 K in order to keep them dry before the experiments. After electrical conductivity experiments, the recovered samples were polished to investigate the microstructures and identify the phase transition products by scanning electronic microscope (SEM) and optical microscope. For the conductivity measurement, the cell design was basically similar to that used in our previous work [*Hu et al.*, 2014, 2015]. The cylindrical sample was sandwiched between two symmetric Ni electrodes, and two nickel-aluminum ($Ni_{97}Al_3$) wires were separately connected to each electrode. Because epidote group minerals host iron in the fully oxidized state [*Franz and Liebscher*, 2004], high oxygen fugacities (equal to or above the hematite-magnetite oxygen buffer) are expected to maximize epidote stability. The oxygen fugacity, therefore, was controlled by using Ni electrodes and its correspondent Ni shielding for the sake of keeping fO_2 close to the Ni-NiO buffer. An Al_2O_3 sleeve was placed outside the sample, and a cylindrical MgO sleeve was put directly in contact with Al_2O_3 sleeve in order to keep a highly insulated electrical environment under experimental conditions. An Ni shielding was used between Al_2O_3 and MgO sleeves and connected to the ground by a wire so as to prevent external electromagnetic disturbance and minimize the thermal gradient of the sample. The heater, made of three layers of stainless steel sheets with a total thickness of 0.5 mm, was installed outside of MgO sleeve. An $Ni_{90}Cr_{10}$-$Ni_{97}Al_3$ thermocouple with a ball head in direct contact with the middle of the sample was used to monitor the temperature of sample. Prior to sample assembly, the pyrophyllite pressure medium with an edge length of 32.5 mm and pyrophyllite end caps were heated at 1023 K for 5 h in order to avoid pyrophyllite dehydration influencing the EC measurements. All other parts were kept at 400 K until they were assembled in order to remove absorbed water. After assembly of the sample, it was kept in a muffle furnace at 473 K until EC measurements.

High-temperature and high-pressure experiments were carried out by using a YJ-3000t multianvil apparatus installed in the Institute of Geochemistry, Chinese Academy of Sciences, Guiyang, China. Complex impedance spectra were measured at temperatures of 573–1273 K and pressures of 0.5–1.5 GPa by a Solartron-1260 Impedance/Gain-Phase Analyzer with the frequency range from 10^{-1} to 10^6 Hz. The applied alternating current voltage was 1 V. For each run, the sample was first compressed to the desired pressure. Under a constant pressure, the sample was slowly heated to 873 K at a rate of 20 K/min and kept at that temperature for 3 h to attain thermal transfer equilibrium and remove the absorbed moisture in the sample assembly. The impedance spectra were collected frequently at 873 K until the sample resistance reached a steady value. The sample was then cooled to 573 K in steps of 50 K, and simultaneously, at each temperature interval, the impedance spectra were measured after the measurement system was stabilized for about 15 min at each temperature interval. The maximum temperature (873 K) during the initial heating-cooling cycles was designed to avoid the decomposition of the sample and ensure the reproducible data before the sample dehydration. During sample dehydration process, the impedance spectra were collected directly without the period of 15 min for stabilizing measurement system at each temperature interval until temperature was raised up to 1273 K in order to investigate the variation of electrical conductivity during sample dehydration process. After no change of resistance at maximum temperature of 1273 K was observed, the impedance spectrum measurements were performed again in the following heating and cooling cycle by the same method as that before sample dehydration. This procedure confirmed the reproducibility of data and minimized the uncertainty of electrical conductivity measurements. Details of the experimental conditions are listed in Table 2.

Since the shapes of impedance arcs in the complex plane exhibited remarkable differences during the different stages of sample, an appropriate equivalent circuit was chosen to model the impedance spectrum in order to determine sample resistance by using a complex nonlinear least squares fitting routine. The electrical conductivity (σ) was then calculated from the sample dimensions and the resistance by using the equation $\sigma = L/SR$, where L and S are the sample length and cross-section area of electrode, respectively, and R is the sample resistance. The sample geometry was checked before and after electrical conductivity

Table 2. The Fitting Parameters for Electrical Conductivity at Different Stages of Sample

Run No.	P (GPa)	T_1 (K) Before Dehydration	T_2 (K) After Breakdown	σ_{01} (S/m)	ΔH_1 (eV)	σ_{02} (S/m)	ΔH_2 (eV)
E11	0.5	523–1023	573–1253	194.98	0.64	103.85	0.91
E22	1.0	523–1073	673–1273	158.05	0.68	84.15	0.94
E31	1.5	523–1073	623–1223	102.40	0.67	48.87	0.92

measurements, and the distortion were found to be so small that they could be ignored during data processing. The uncertainty in temperature due to the thermal gradient along the length of sample cell was less than 5 K. The uncertainty in pressure in the sample cell was lower than 0.1 GPa according to the pressure calibration in YJ-3000t multianvil apparatus [*Shan et al.*, 2007]. Therefore, the total uncertainty of electrical conductivity, including impedance spectra fitting and temperature, was no more than 5%.

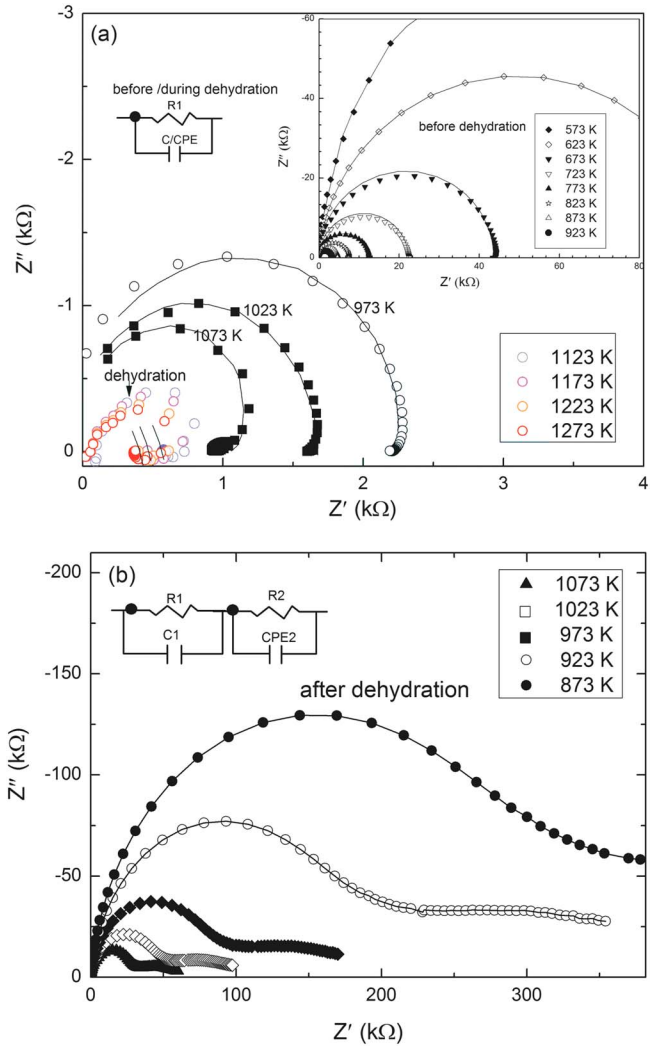

Figure 2. Representative complex spectra at different stages of the sample. (a) Before sample dehydration (below 1073 K), the spectra show the ideal semicircle arcs in the complex plane, which represents the bulk conduction of single crystal epidote. During sample dehydration process, the impedance arcs marked by colored symbols show that the inductive loop in the low-frequency regime reflected the occurrence of dehydration reaction. An equivalent circuit of a single RC/CPE in parallel is used to fit these impedance arcs. (b) After sample dehydration, the grain boundary arcs are well developed in the low-frequency range owing to sample breakdown. The solid lines represent the fitting results by the equivalent circuit.

3. Results

Representative impedance spectra at different stages of heating and cooling at 0.5 GPa are displayed in Figure 2. At temperatures below 1073 K (before sample dehydration), the spectra show a Debye semicircle in the complex impedance plane over the whole frequency range with a center that falls on the real axis. The semicircular arc represents the bulk conduction of sample because there are no grain boundaries in the single crystal sample of epidote, and hence, it can be fitted by a parallel resistance-capacitance equivalent circuit to determine the sample resistance [*Huebner and Dillenburg*, 1995]. The diameters of the semicircular arcs gradually decrease with increasing temperature, implying a decrease of resistance and an increase in electrical conductivity of sample. At 1123 K, the onset of sample dehydration, the impedance arcs remarkably shrink as indicated by the colored symbols in Figure 3a, implying the slope of electrical conductivity changes ~1123 K. Meanwhile, the extent of variation of impedance arcs at temperatures above 1123 K becomes smaller, reflecting a gentle increase in electrical conductivity. At high temperatures during the dehydration process, the impedance arcs in the low-frequency regime indicate the positive Z'' of the presence of the inductive loop, which is related to

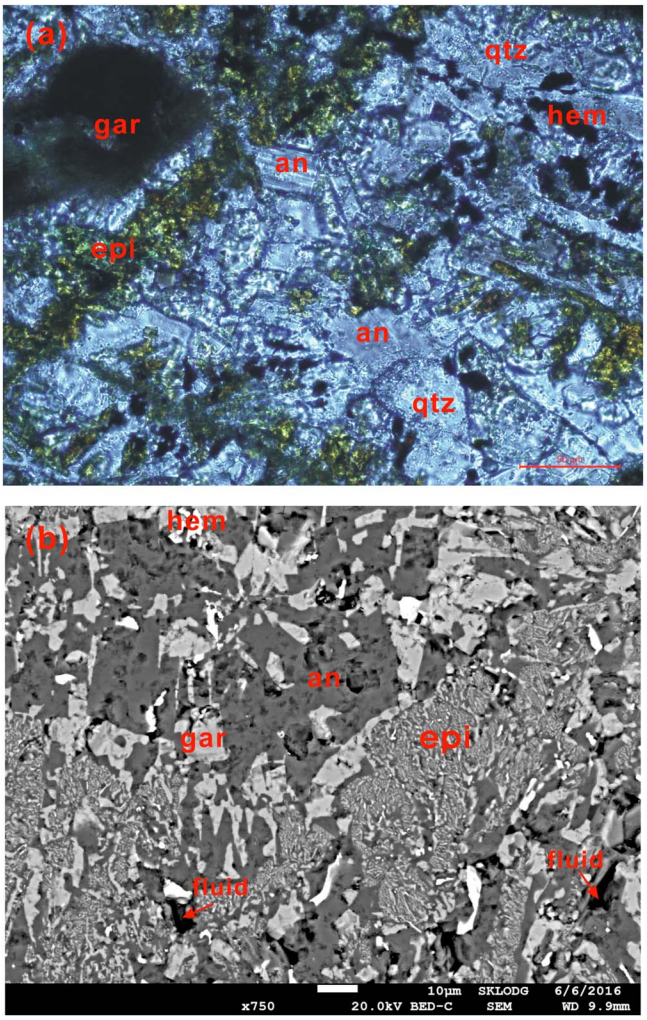

Figure 3. (a) Optical microscope image and (b) SEM image of the recovered sample after conductivity measurements. The presence of voids (dark-gray regions) showed in the SEM image corresponds to the presence of aqueous fluid preserved during high *P–T* experiments. Abbreviations: an, anorthite; epi, epidote; hem, hematite; qtz, quartz; grt, garnet.

electrode-fluid reaction at the sample electrode interface, as reported previously [*Bai and Conway*, 1991; *Macdonald*, 1978]. Therefore, the inductive loop that appears at low frequencies reflects the occurrence of dehydration reaction, as are also observed for other hydrous minerals such as talc [*Wang and Karato*, 2013] and chlorite [*Manthilake et al.*, 2016]. After dehydration, the impedance spectra in the lower frequency range are remarkably developed, which is usually attributed to the contribution of a grain boundary component to the sample resistance [*Roberts and Tyburczy*, 1993; *Dai et al.*, 2013]. The appearance of grain boundary impedance arcs reflects the breakdown of the single crystal sample and the formation of new phases that are confirmed by using images produced with an SEM and optical microscope for the recovered sample, as shown in Figure 3.

The temperature dependence of electrical conductivity for silicate minerals is usually expressed according to the Arrhenius relationship:

$$\sigma = \sigma_0 \left(-\frac{\Delta H}{kT} \right), \qquad (1)$$

where σ_0 is a pre-exponential factor (S/m), k is the Boltzmann constant (eV/K), T is the absolute temperature (K), and ΔH is the activation enthalpy (eV), which can be defined as a function of pressure (P) and is expressed by $\Delta H = \Delta E_0 + P\Delta V$, where ΔE and ΔV are the activation energy and the activation volume, respectively. The examples of electrical conductivity in different heating and cooling cycles at 1.5 GPa and the conductivity data at 0.5–1.5 GPa are illustrated in Figures 4 and 5, respectively. As the plot of electrical conductivity versus temperature shows different slopes at different stages of sample heating, the data were separately fitted by the Arrhenius formula. Accordingly, the fitting parameters from equation (1) are summarized in Table 2.

The electrical conductivity measurements were carried out in the several heating/cooling cycles at 0.5–1.5 GPa, and similar features are displayed as Figure 4. In the first cooling and second heating cycle, the logarithmic conductivity increases with increasing temperature and a good reproducibility of data was acquired before sample dehydration (<873 K). Once the sample was heated to ~1073 K, a noticeably weak dependence of electrical conductivity on temperature was observed, and when the sample was kept at the maximum temperature of 1273 K, electrical conductivity displayed the remarkable decrease, reflecting the progressive dehydration of the sample and the simultaneously but gradual escape of the aqueous fluid from the sample cell. The dehydration temperature (~1073) roughly corresponds to the breakdown of epidote into a multiphase assemblage of grossular garnet, anorthite, quartz, hematite, and fluid, which is in consistency with the results of phase equilibrium experiments with epidote by *Poli and Schmidt* [2004].

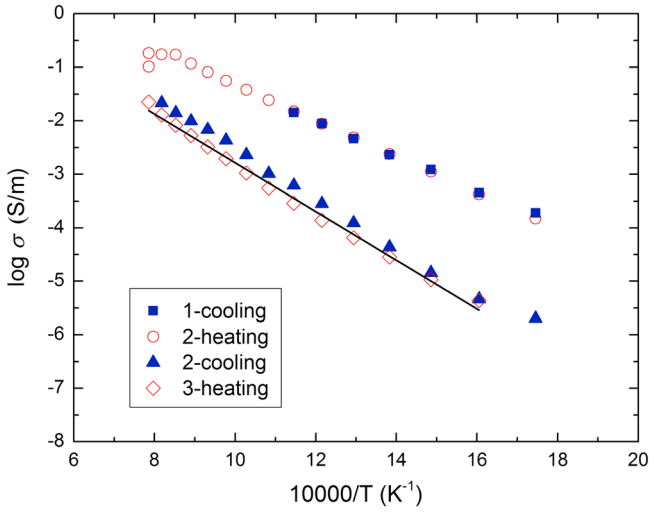

Figure 4. Electrical conductivities of epidote as a function of reciprocal temperatures along different heating/cooling cycles. The conductivities in the first cooling and second heating below 873 K are reproducible, and after the sample dehydration at high temperature regimes, the trace of the second cooling path is almost consistent with that of the third heating path.

After sample dehydration, relatively low electrical conductivity was yielded in the following cooling and heating cycles and the data demonstrated good reproducibility. Accordingly, relatively high activation enthalpies are obtained with the value of about 0.90 eV. The incomplete breakdown of the epidote sample was investigated after EC experiments by images of optical microscope (Figure 3a) and SEM (Figure 3b).

The electrical conductivities (Figure 5) at different pressures also demonstrate similar features with three different stages of sample as shown in Figure 4. The distinguishable variation of the electrical conductivity was displayed in the heating path ~1073 K, which indicates the occurrence of sample dehydration. After annealing at the maximum temperature of 1273 K, the reproducibility of electrical conductivity implies the formation of a mineral assemblage with relatively low electrical conductivity. As illustrated in Figure 5, the influence of pressure on the electrical conductivity is relatively weak compared with temperature. There is

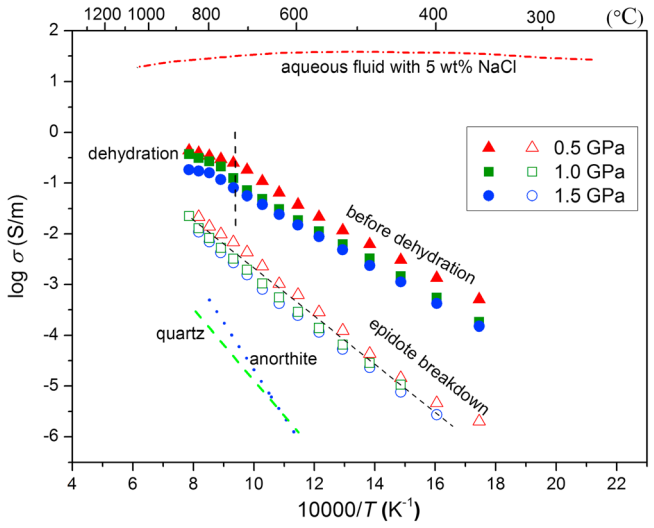

Figure 5. The logarithm of electrical conductivity of epidote as a function of reciprocal temperature at 0.5–1.5 GPa. Data from different pressures show good reproducibility, and the moderate increase of EC is observed when the sample dehydration happened ~1073 K. The decrease of EC by more than 1 order of magnitude is also observed after the breakdown of epidote at different pressures. The orange dash-dotted line is the EC data of aqueous fluid with 5 wt % NaCl from *Sinmyo and Keppler* [2017]. The blue dotted line and green dashed line are the EC data of polycrystalline anorthite and quartz from *Hu et al.* [2015] and *Bagdassarov and Delépine* [2004], respectively.

a tendency for the effect of pressure on electrical conductivity of epidote to become small as pressures increase (Figure 5), and even at low temperature, the electrical conductivities overlap at 1.0 GPa and 1.5 GPa. Meanwhile, the activation enthalpies at various pressures in the same temperature range demonstrate only slight discrepancy as shown in Table 2. As a consequence, the effect of pressure on electrical conductivity is not considered in the following discussion sections.

4. Discussions

4.1. Conduction Mechanism

Since several distinct types of electrical conductivity/temperature dependences on the Arrhenius plot in Figure 5 were observed in the sample heating and cooling cycles, different conduction mechanisms can be identified and operate individually in the different stages of sample. At temperatures below ~1073 K (before sample dehydration), the measured high conductivities and low activation enthalpies (~0.70 eV) at pressures of 0.5–1.5 GPa can probably be attributed to the H_2O in sample, or in other words, hydrogen-related defect (H) as the main charge carriers may dominate the conduction mechanism. For the Fe-bearing nominally hydrous minerals, proton (H) conduction and small polaron conduction by the hopping of electron holes between Fe^{2+} and $Fe^{3+}$are commonly considered to be two representative mechanisms of charge transport before the dehydration stage. However, the relatively low activation energies (~0.6–0.8 eV) reported for talc, serpentinite, and brucite [*Fuji-ta et al.*, 2007; *Guo et al.*, 2011; *Guo and Yoshino*, 2014] are often attributed to the migration of proton owing to its small ion radius and highly mobility, although these minerals contain small amounts of iron. In contrast, for Fe-bearing nominally anhydrous minerals, the conduction by the hopping of small polaron is often characterized by relatively high activation energy, which depends on iron concentration in sample [*Dai and Karato*, 2009; *Poe et al.*, 2010; *Yang et al.*, 2012; *Yoshino et al.*, 2012]. For Fe-bearing nominally hydrous minerals, the activation energy for small polaron conduction is also high (~1.3 eV), e.g., antigorite [*Reynard et al.*, 2011] and pyrophyllite [*Hicks and Secco*, 1997], which is similar to the situation for Fe-bearing nominally anhydrous minerals. Despite that our sample is iron-rich epidote with Fe_2O_3 content of ~12.25 wt % (Table 1), the replacement of Al^{3+} by Fe^{3+} ion increases the O–O distance which results in a weakening of hydrogen bond with increasing Fe content reported by *Kvick et al.* [1988]. Thus, the low ΔH (~0.70 eV) and high electrical conductivity before sample dehydration in this study may have been the result of a significant contribution of proton conduction.

At temperatures above 1073 K, the presence of aqueous fluids released during sample dehydration as well as the simultaneous escape of fluids from sample cell caused a discontinuous variation in electrical conductivity. We propose that the bulk electrical conductivity was dominated by the water fluid with very low or no salinity, because as shown in Figure 5, aqueous fluids with 5 wt % NaCl have extremely high conductivity value [*Sinmyo and Keppler*, 2017]. After a long duration at the highest temperature of 1273 K, the reproducible low electrical conductivity in final cooling/heating cycles and relatively high activation enthalpy (~0.90 eV) are obtained. According to SEM and optical microscope images shown in Figure 3, massive anorthite and quartz form an interconnected network as matrix in the sample and the residual epidote distributes as isolated shapes in the grain boundary; consequently, the bulk conductivity of the sample is most likely dominated by the weak conductive anorthite and quartz. However, according to the electrical conductivity data of polycrystalline quartz [*Bagdassarov and Delépine*, 2004] and anorthite [*Hu et al.*, 2015] as shown in Figure 5, both of them have restively low electrical conductivity and higher activation enthalpies (~1.40 eV for quartz and 1.90 eV for anorthite) compared to the present value (0.90 eV). Consequently, it is expected that the presence of a small amount of aqueous fluid continuously released from residual epidote causes an enhancement of electrical conductivity and the decrease in activation enthalpy. Aqueous fluids from the residual epidote located in grain boundary presumably facilitated the migration of charge carriers in solid matrix. Therefore, the bulk conductivity of the sample was probably controlled by the coexisting solid phases (quartz and anorthite) and aqueous fluids existing in the grain boundary.

4.2. Comparisons With Previous Data of Hydrous Minerals

Previous conductivity data for epidote at high temperature and high pressure are unfortunately unavailable. However, the EC data for most of other nominally hydrous minerals in subduction zones have been widely reported [*Guo et al.*, 2011; *Reynard et al.*, 2011; *Wang et al.*, 2012; *Wang and Karato*, 2013; *Manthilake et al.*, 2015, 2016; *Li et al.*, 2016]. Comparisons with these data therefore are therefore important in explaining

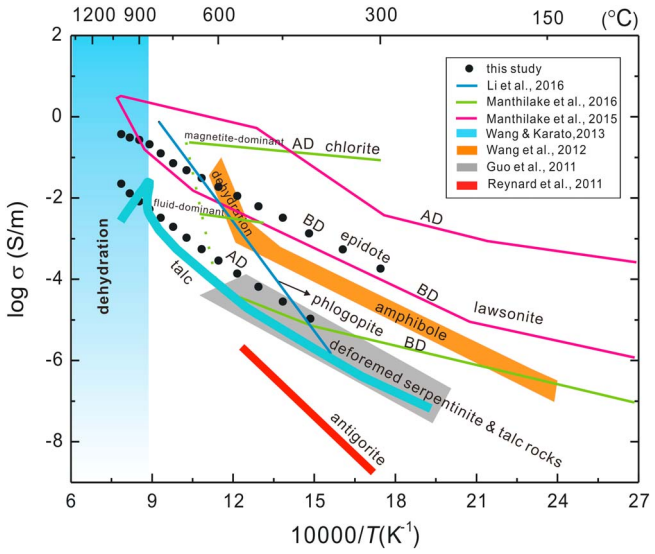

Figure 6. Electrical conductivity of epidote and comparison with available data on hydrous minerals. The thick red line represents a result of antigorite [*Reynard et al.*, 2011]. The gray field denotes the deformed serpentinites and talc rocks [*Guo et al.*, 2011]. The thick light blue and orange lines indicate talc aggregates and amphibole-bearing rocks, respectively [*Wang et al.*, 2012; *Wang and Karato*, 2013]. The thin pink and green lines illustrate lawsonite and chlorite, respectively [*Manthilake et al.*, 2015, 2016]. The dark blue line represents phlogopite [*Li et al.*, 2016]. Abbreviation: BD, before dehydration; AD, after dehydration.

the high conductivity anomalies in the subduction zones. The noticeable discrepancies exist among the results of these different experiments as shown in Figure 6.

Reynard et al. [2011] reported the electrical conductivities of three natural antigorites at pressures of up to 5 GPa and temperatures of up to 798 K, and the low electrical conductivities ($<10^{-4}$ S/m) as shown in Figure 6 are obviously lower than our results. They concluded that electrical conductivity of antigorite could not account for the high conductivities observed in the mantle wedge, and the electrical conductivity in the hydrated mantle wedge is only sensitive to fluid content and salinity, not to serpentinization. *Guo et al.* [2011] measured the electrical conductivity measurements of deformed natural talc rocks and serpentinites at 500–1000 K and 3 GPa, yielding the low electrical conductivities that are similar to the present results at low temperatures after sample dehydration. Therefore, the anomalously high conductor in both warm and cold subduction zones cannot be explained by the presence of talc and serpentinites. However, the activation enthalpies (0.59–0.75 eV) for deformed serpentinites and talc rocks reported by *Guo et al.* [2011] are generally consistent with our data (~0.70 eV) before sample dehydration, and in both studies, the structural water conduction is also proposed to be dominant conduction mechanism.

Wang and Karato [2013] performed electrical conductivity experiments of talc aggregates before and after dehydration at 0.5 GPa, and EC values are much lower than those of our results before and during dehydration, although *Wang and Karato* [2013] did observe an abrupt increase in electrical conductivity during dehydration process. They concluded that the electrical conductivity of talc is possibly dominated by ferric iron both before and after dehydration, rather than proton (H) or aqueous fluid. Similarly, they also concluded that the high activation enthalpy and enhanced conductivity of amphibole during the dehydration process were not caused by the conductive fluids but by the dissociation of OH^- into hydrogen and oxygen associated with the oxidation of iron [*Wang et al.*, 2012]. There are inconsistencies in their results and ours with regard to the contribution of aqueous fluids to the EC. The dehydration temperature of amphibole observed by *Wang et al.* [2012] is much lower than that of epidote observed in this study, and this is consistent with experimental studies that revealed that epidote minerals have huge stability fields exceeding the field of amphibole stability (70–80 km) [*Poli and Schmidt*, 1995, 1998; *Schmidt and Poli*, 1998].

Manthilake et al. [2015] conducted the electrical conductivity measurement on lawsonite at 7 GPa and temperatures of 298–1320 K, reporting the sharp increase in conductivity when exceeding the dehydration temperature of ~1258 K. The electrical conductivity of lawsonite after dehydration is much higher than our results in a similar temperature range, although both the lawsonite and epidote have similar electrical conductivity values before dehydration. *Manthilake et al.* [2015] attributed the increase in electrical conductivity to the highly conductive fluid released during its dehydration, which is similar to our conclusion for epidote. More recently, the electrical conductivity of natural chlorite under conditions prevailing the subduction zone was determined by *Manthilake et al.* [2016]. In their study, the two distinct enhancements of conductivity after chlorite dehydration were attributed to the release of aqueous fluids and interconnected highly conductive magnetite, respectively. The lower electrical conductivities of aqueous fluid and higher conductivity

of impure magnetite formed after the breakdown of chlorite are inconsistent with our results before and after epidote dehydration. Furthermore, their results demonstrated that aqueous fluids alone cannot interpret the anomalous high conductivity in the mantle wedge, but the interconnected conductive impure magnetite with 14 vol % can do. Anisotropic electrical conductivity data of phlogopite from *Li et al.* [2016] revealed a large activation energy for the geometrical mean of the conductivity (1.78 eV), which was attributed to the probably K^+ and F^- conduction. Accordingly, *Li et al.* [2016] suggested that the highly conductive anomalies above subduction zones or in normal shields could be caused by a regional enrichment of K- and F-rich phlogopites. The electrical conductivities of phlogopite are higher than those we observed for epidote in the high temperature regime.

4.3. Implications for Highly Conductivity Anomalies in Subduction Zones

According to the laboratory conductivity data for important hydrous minerals in the subduction zone (Figure 6), the dehydration of some hydrous minerals such as amphibole [*Wang et al.*, 2012] and talc [*Wang and Karato*, 2013] cannot be the cause of the anomalous high conductivity in spite of the presence of aqueous fluids released during dehydration reaction. On the other hand, it has been suggested that the high conductive accessory minerals such as oxides (magnetite), phlogopite, and sulfides (or saline fluids) could account for the high conductivity anomalies in subduction zones by the conductivity model of two phase medium consisting of a resistive matrix and those conductive materials [*Reynard et al.*, 2011; *Li et al.*, 2016; *Manthilake et al.*, 2016; *Sakuma and Ichiki*, 2016]. These results are somewhat efficient for the interpretation of some regional highly conductive anomalies, but not consistent with the widespread interpretation of highly conductive zones in terms of partial melting or the accumulation of free fluids [*Ichiki et al.*, 2000; *Soyer and Unsworth*, 2006; *Worzewski et al.*, 2011; *Evans et al.*, 2014; *McGary et al.*, 2014; *Pommier*, 2014]. Since the thermal structure of a subduction zone determines the depth at which the hydrous minerals become dehydrated in the subducting slab, therefore, if regardless of the complexity and diversity of thermal and petrological structure in different subduction zones, a single high conductivity mechanism observed from experimental conductivity study on a single hydrous mineral can hardly explain the widespread highly conductive anomalies in subduction zones. Accordingly, the laboratory electrical conductivity data on geomaterials, together with petrological results, are generally required to explain the field electromagnetic data for a clear map of composition, temperature, and geological processes.

Based on the typical mineralogy and thermal model of a subduction zone given by *Schmidt and Poli* [1998] as shown in Figure 7a, the depth of the release of water from the subducting slab is related to the thermal stability of various hydrous minerals and thermal structure of the subduction zones. Epidote forms throughout greenschist facies and reaches up to 35 vol % in epidote-blueschist facies. The transition from blueschist to eclogite facies occurs via the consumption of epidote; thus, this mineral is the ultimate fluid source in mafic rock compositions in an oceanic crust subducting at intermediate temperatures [*Poli and Schmidt*, 2004]. The highly conductive anomalies shown in Figure 7a in the mantle wedge (~70–120 km) are widely observed by magnetotelluric imaging of the subduction zones [*Soyer and Unsworth*, 2006; *Evans et al.*, 2014; *McGary et al.*, 2014].The enhanced conductivity in these zones is commonly interpreted as the presence of free fluids released from the underlying subducting crust, although partial melting of the mantle wedge is another possible way of explaining the deep high conductivity region of mantle wedge, especially for the young and hot subduction zones. Consequently, aqueous fluids derived from the dehydration of zoisite/epidote in subducting slab at depths below 70 km shown in Figure 7a may make a significant contribution to deep highly conductive anomalies in the mantle wedge.

To explain the deep highly electrical conductors in the mantle wedge, the different thermal structures along subduction zones for cool and hot subduction need to be considered, because electrical conductivity is particularly sensitive to temperature. The typical hot and cool thermal models for a slab surface, derived respectively from Central Cascadia subduction zones and central New Zealand subduction zones, are adopted and shown in Figure 7b [*Syracuse et al.*, 2010], in order to establish the laboratory-based conductivity-depth profile by electrical conductivity data of epidote in this study and the data for dry eclogite from *Dai et al.* [2016]. The thermal structure of the wedge from *Currie et al.* [2004] was also selected, together with the SEO3 model for dry olivine from *Constable* [2006]. These results, along with the high conductivity zone in mantle wedge at depths of ~70–120 km, are shown in Figure 7b.

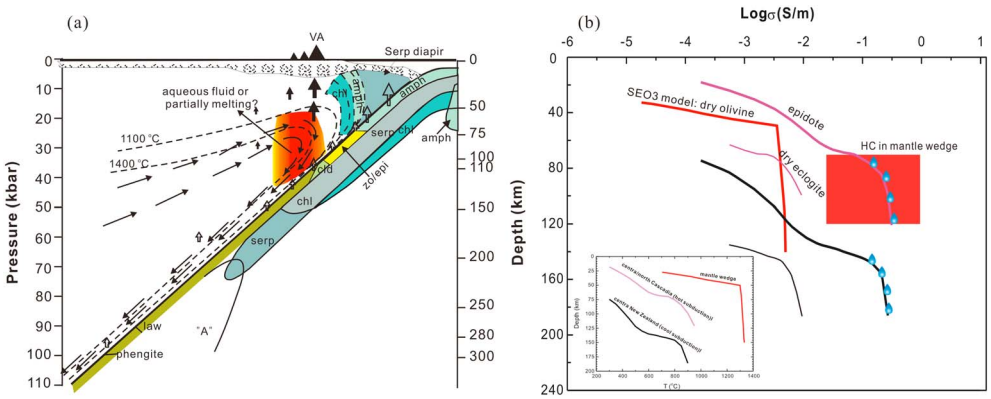

Figure 7. (a) Mineralogical model of the subduction zone is referred from *Schmidt and Poli* [1998]. The red regions in the mantle wedge are the anomalous high conductivity zones extensively detected by magnetotelluric and seismic velocity surveys; (b) conductivity-depth profiles established from the data of epidote in this study, dry eclogite from *Dai et al.* [2016] and SEO3 model for dry olivine from *Constable* [2006] based on the thermal structure of subduction slab in the typical hot (Central Cascadia subduction zones) and cool (central New Zealand subduction zone) subduction zones [*Syracuse et al.*, 2010], and the mantle wedge [*Currie et al.*, 2004], respectively, which are shown in the inset. The thick solid purple black lines represent EC profile from the present data before epidote dehydration in hot and cool subduction slabs, respectively. The thin solid purple and black lines denote EC profile from the data of dry eclogite in hot and cool subduction slabs, respectively. The solid red line indicates the SEO3 model for dry olivine in the mantle wedge. The red rectangle shows the HCZ in the mantle wedge at depths of ~70–120 km. The waterdrops refer to the epidote dehydration process. Abbreviations: a, phase a; amph, amphibole; chl, chlorite; cld, chloritoid; serp, serpentine; law, lawsonite; zo, zoisite; epi, epidote.

A typical highly conductivity region in the mantle wedge of the Cascadia hot subduction system was investigated at depths of ~80–90 km by magnetotelluric method [*Soyer and Unsworth*, 2006; *Evans et al.*, 2014; *McGary et al.*, 2014]. According to the thermal model of the slab interface, the depth of initial occurrence of epidote dehydration reaction (marked by waterdrops on the thick solid purple line in Figure 7b) is just within the range of 80–90 km, which is consistent with the depth of highly conductive anomaly. Aqueous fluids from epidote dehydration reaction would migrate upward into the overlying mantle wedge and could cause extensive accumulation in the overlying mantle; partial melting may also be triggered in the core of the converting mantle wedge through reducing the melting temperature. However, partial melting can explain the high conductor only if the temperature is high enough ($>$1473 K) in the hot core of the mantle wedge, based on the electrical conductivity of hydrous basaltic melt [*Ni et al.*, 2011]. The temperature of the high conductor in the mantle wedge of central Cascadia subduction is in the range of ~1373–1673 K as indicated by *van Keken et al.* [2011] and therefore partial melting of the mantle-wedge peridotite, triggered by the involvement of aqueous fluid released from epidote dehydration, may be responsible for the high conductivity in the hot core of this mantle wedge, because dry olivine has a low electrical conductivity value (Figure 7b). In addition, the electrical conductivity of epidote during dehydration falls in the range of high conductors (~0.1–1 S/m) in the mantle wedge, and it is likely, therefore, that poorly conductive eclogite accounts for the highly conductive anomaly of the slab interface if a certain amount of residual epidote exists and interconnects in eclogite during the transition from blueschist to eclogite facies. Consequently, the deep highly conductive anomalies at depths of more than 80 km in Cascadia subduction zone can be interpreted as a consequence of free fluids from continuously progressive dehydration of epidote.

In the case of the representative cool subduction zone in New Zealand, a conductive zone at depths below 100 km has been observed by MT sounding inversion, attributed to the amphibole-zoisite breakdown at 75–100 km depth in the subducting slab [*Wannamaker et al.*, 2009]. However, owing to the low thermal gradient of the slab surface in New Zealand [*Syracuse et al.*, 2010], the depth where the dehydration reaction of epidote initially occurs is about 140 km (marked by waterdrops on the thick solid black line in Figure 7b), which is much deeper than that of high conductive region. The depth of the occurrence of epidote dehydration in cool subduction zone is consistent with that from petrological studies that reported that the blueschist-eclogite transformation may release large amounts of H_2O by the breakdown reaction of glaucophane, clinozoisite, and/or lawsonite at depths below 100 km [*Liu et al.*, 1996]. Therefore, fluids released from the dehydration of epidote are less efficient to account for the high conductive region in the deep mantle

wedge at depth greater than 100 km. In contrast, amphibole would make a significant contribution to provide aqueous fluids to the mantle wedge, since the dehydration of amphibole occurs at relatively shallow depths (65–90 km) [*Schmidt and Poli*, 1998]. In summary, the present results suggest that the fluid released during epidote dehydration could make a significant contribution to the origin of deep anomalous highly conductivity zones in mantle wedge below 70 km, particularly for the hot subduction zones.

5. Conclusions

In this study, the electrical conductivities of natural epidote as a function of temperature (573–1273 K) and pressure (0.5–1.5 GPa) were measured by AC Impedance/Gain-Phase Analyzer. The pressure dependence on the electrical conductivity was relatively weak compared to temperature and tends to be smaller with increasing pressure. The dehydration process of epidote was investigated at elevated temperatures (>1073 K), and the maximum conductivity reaches up to ~1 S/m at 1273 K, but the discontinuous variation of electrical conductivity occurs in high temperature regimes, which can be ascribed to the presence of aqueous fluid in sample and the simultaneous escape of fluids from sample cell. Incompletion dehydration and residual epidote were investigated after sample dehydration, and the reproducible electrical conductivity decreases noticeably by almost a log unit under similar conditions to the dehydration process. The lower conductivity after sample dehydration is presumably dominated by the coexisting high resistive mineral assemblages (anorthite and quartz) and aqueous fluids from the residual epidote.

In a combination of the thermal and petrologic structure in subduction zones, the conductivity-depth profiles in the typical hot and cold subduction zones are respectively established based on our data in order to account for the high conductivity anomalies at depths blow 70 km in the deep mantle wedge. Our results suggests that the fluids released from epidote dehydration make a significant contribution to the highly conductive anomalies of the deep mantle wedge, particularly in the hot subduction zones. This occurs not only in mantle wedge near the slab interface at depths of 70–120 km but also at the hot corner of the mantle wedge into which fluids migrate upward, resulting in partial melting.

Acknowledgments

We thank the editor of André Revil, associate editor, and three anonymous reviewers for their very valuable and enlightened comments and suggestions, which greatly improve the manuscript. We are also grateful to Wenqin Zheng and Shaohua Dong for their assistance of the use of microelectron probe and scanning electronic microscope, respectively. The data for this paper are available from the author upon request (huhaiying@vip.gyig.ac.cn). This research was financially supported by the Strategic Priority Research Program (B) of the Chinese Academy of Sciences (XDB 18010401), the Key Research Projects of the Frontier Science of the Chinese Academy of Sciences (QYZDB-SSW-DQC009), the "135" Program of the Institute of Geochemistry of CAS, Hundred Talents Program of CAS, NSF of China (41474078, 41304068, and 41174079), and the Open Foundation of Institute of Geology and Geophysics of CAS.

References

Apted, M. J., and J. Liou (1983), Phase relations among greenschist, epidote-amphibolite, and amphibolite in a basaltic system, *Am. J. Sci.*, *283*, 328–354.

Bagdassarov, N. S., and N. Delépine (2004), α-β inversion in quartz from low frequency electrical impedance spectroscopy, *J. Phys. Chem. Solids*, *65*, 1517–1526.

Bai, L., and B. Conway (1991), AC impedance of faradaic reactions involving electrosorbed intermediates: Examination of conditions leading to pseudoinductive behavior represented in three-dimensional impedance spectroscopy diagrams, *J. Electrochem. Soc.*, *138*(10), 2897–2907.

Chen, T., and R. W. Clayton (2009), Seismic attenuation structure in central Mexico: Image of a focused high-attenuation zone in the mantle wedge, *J. Geophys. Res.*, *114*, B07304, doi:10.1029/2008JB005964.

Constable, S. (2006), SEO3: A new model of olivine electrical conductivity, *Geophys. J. Int.*, *166*(1), 435–437.

Currie, C. A., K. Wang, R. D. Hyndman, and J. He (2004), The thermal effects of steady-state slab-driven mantle flow above a subducting plate: The Cascadia subduction zone and backarc, *Earth Planet. Sci. Lett.*, *223*(1–2), 35–48.

Dai, L., and S. Karato (2009), Electrical conductivity of pyrope-rich garnet at high temperature and high pressure, *Phys. Earth Planet. Inter.*, *176*, 83–88.

Dai, L., H. Li, H. Hu, J. Jiang, K. Hui, and S. Shan (2013), Electrical conductivity of $Alm_{82}Py_{15}Grs_3$ almandine-rich garnet determined by impedance spectroscopy at high temperatures and high pressures, *Tectonophysics*, *608*, 1086–1093.

Dai, L., H. Hu, H. Li, L. Wu, K. Hui, J. Jiang, and W. Sun (2016), Influence of temperature, pressure, and oxygen fugacity on the electrical conductivity of dry eclogite, and geophysical implications, *Geochem., Geophys., Geosyst.*, *17*, 2394–2407, doi:10.1002/2016GC006282.

Evans, R. L., P. E. Wannamaker, R. S. McGary, and J. Elsenbeck (2014), Electrical structure of the central Cascadia subduction zone: The EMSLAB Lincoln Line revisited, *Earth Planet. Sci. Lett.*, *402*, 265–274.

Franz, G., and J. Selyerstone (1992), An empirical phase diagram for the clinozoisite-zoisite transformation in the system $Ca_2Al_3Si_3O_{12}(OH)$-$Ca_2Al_2Fe^{3+}Si_3O_{12}(OH)$, *Am. Mineral.*, *77*, 631–642.

Franz, G., and A. Liebscher (2004), Physical and chemical properties of the epidote minerals—An introduction, *Rev. Mineral. Geochem.*, *56*(1), 1–81.

Fuji-ta, K., T. Katsura, T. Matsuzaki, and M. Ichiki (2007), Electrical conductivity measurements of brucite under crustal pressure and temperature conditions, *Earth Planets Space*, *59*(6), 645–648.

Grodzicki, M., S. Heuss-Assbichler, and G. Amthauer (2001), Mössbauer investigations and molecular orbital calculations on epidote, *Phys. Chem. Miner.*, *28*(9), 675–681.

Guo, X., and T. Yoshino (2014), Pressure-induced enhancement of proton conduction in brucite, *Geophys. Res. Lett.*, *41*, 813–819, doi:10.1002/2013GL058627.

Guo, X., T. Yoshino, and I. Katayama (2011), Electrical conductivity anisotropy of deformed talc rocks and serpentinites at 3 GPa, *Phys. Earth Planet. Inter.*, *188*(1), 69–81.

Hicks, T. L., and R. A. Secco (1997), Dehydration and decomposition of pyrophyllite at high pressures: Electrical conductivity and X-ray diffraction studies to 5 GPa, *Can. J. Earth Sci.*, *34*(6), 875–882.

Hu, H., L. Dai, H. Li, J. Jiang, and K. Hui (2014), Electrical conductivity of K-feldspar at high temperature and high pressure, *Mineral. Petrol.*, *108*(5), 609–618.
Hu, H., L. Dai, H. Li, K. Hui, and J. Li (2015), Temperature and pressure dependence of electrical conductivity in synthetic anorthite, *Solid State Ionics*, *276*, 136–141.
Huebner, J. S., and R. G. Dillenburg (1995), Impedance spectra of hot, dry silicate minerals and rock: Qualitative interpretation of spectra, *Am. Mineral.*, *80*(1–2), 46–64.
Ichiki, M., N. Sumitomo, and T. Kagiyama (2000), Resistivity structure of high-angle subduction zone in the southern Kyushu district, southwestern Japan, *Earth Planets Space*, *52*(8), 539–548.
Kvick, Å., J. Pluth, J. Richardson, and J. Smith (1988), The ferric ion distribution and hydrogen bonding in epidote: A neutron diffraction study at 15 K, *Acta Crystallogr., Sect. B: Struct. Sci.*, *44*(4), 351–355.
Li, Y., X. Yang, J. H. Yu, and Y. F. Cai (2016), Unusually high electrical conductivity of phlogopite: The possible role of fluorine and geophysical implications, *Contrib. Mineral. Petrol.*, *171*(4), 1–11.
Liu, J., S. Bohlen, and W. Ernst (1996), Stability of hydrous phases in subducting oceanic crust, *Earth Planet. Sci. Lett.*, *143*(1), 161–171.
Macdonald, D. D. (1978), A method for estimating impedance parameters for electrochemical systems that exhibit pseudoinductance, *J. Electrochem. Soc.*, *125*(12), 2062–2064.
Manthilake, G., M. Mookherjee, N. Bolfan-Casanova, and D. Andrault (2015), Electrical conductivity of lawsonite and dehydrating fluids at high pressures and temperatures, *Geophys. Res. Lett.*, *42*, 7398–7405, doi:10.1002/2015GL064804.
Manthilake, G., N. Bolfan-Casanova, D. Novella, M. Mookherjee, and D. Andrault (2016), Dehydration of chlorite explains anomalously high electrical conductivity in the mantle wedges, *Sci. Adv.*, *2*(5), e1501631, doi:10.1126/sciadv.1501631.
McGary, R. S., R. L. Evans, P. E. Wannamaker, J. Elsenbeck, and S. Rondenay (2014), Pathway from subducting slab to surface for melt and fluids beneath Mount Rainier, *Nature*, *511*(7509), 338–340.
Ni, H., H. Keppler, and H. Behrens (2011), Electrical conductivity of hydrous basaltic melts: Implications for partial melting in the upper mantle, *Contrib. Mineral. Petrol.*, *162*(3), 637–650.
Ono, S. (1998), Stability limits of hydrous minerals in sediment and mid-ocean ridge basalt compositions: Implications for water transport in subduction zones, *J. Geophys. Res.*, *103*(B8), 18,253–18,267, doi:10.1029/98JB01351.
Poe, B., C. Romano, F. Nestola, and J. Smyth (2010), Electrical conductivity anisotropy of dry and hydrous olivine at 8 GPa, *Phys. Earth Planet. Inter.*, *181*, 103–111.
Poli, S., and M. W. Schmidt (1995), H_2O transport and release in subduction zones: Experimental constraints on basaltic and andesitic systems, *J. Geophys. Res.*, *100*(B11), 22,299–22,314.
Poli, S., and M. Schmidt (1998), The high-pressure stability of zoisite and phase relationships of zoisite-bearing assemblages, *Contrib. Mineral. Petrol.*, *130*(2), 162–175.
Poli, S., and M. W. Schmidt (2004), Experimental subsolidus studies on epidote minerals, *Rev. Mineral. Geochem.*, *56*(1), 171–195.
Pommier, A. (2014), Geophysical assessment of migration and storage conditions of fluids in subduction zones, *Earth Planets Space*, *66*, 38, doi:10.1186/1880-5981-66-38.
Pozgay, S. H., D. A. Wiens, J. A. Conder, H. Shiobara, and H. Sugioka (2009), Seismic attenuation tomography of the Mariana subduction system: Implications for thermal structure, volatile distribution, and slow spreading dynamics, *Geochem., Geophys., Geosyst.*, *10*, Q04X05, doi:10.1029/2008GC002313.
Reynard, B., K. Mibe, and B. V. de Moortèle (2011), Electrical conductivity of the serpentinized mantle and fluid flow in subduction zones, *Earth Planet. Sci. Lett.*, *307*, 387–394.
Roberts, J. J., and J. A. Tyburczy (1993), Impedance spectroscopy of single and polycrystalline olivine: Evidence for grain boundary transport, *Phys. Chem. Miner.*, *20*, 19–26.
Sakuma, H., and M. Ichiki (2016), Electrical conductivity of NaCl-H_2O fluid in the crust, *J. Geophys. Res. Solid Earth*, *121*, 577–594, doi:10.1002/2015JB012219.
Schmidt, M. W., and S. Poli (1998), Experimentally based water budgets for dehydrating slabs and consequences for arc magma generation, *Earth Planet. Sci. Lett.*, *163*(1), 361–379.
Shan, S., R. Wang, J. Guo, and H. Li (2007), Pressure calibration for the sample cell of YJ-3000t multi-anvil press at high-temperature and high-pressure, *Chin. J. High Press. Phys.*, *21*, 367–372.
Sinmyo, R., and H. Keppler (2017), Electrical conductivity of NaCl-bearing aqueous fluids to 600°C and 1 GPa, *Contrib. Mineral. Petrol.*, *172*(1), 4, doi:10.1007/s00410-016-1323-z.
Soyer, W., and M. Unsworth (2006), Deep electrical structure of the northern Cascadia (British Columbia, Canada) subduction zone: Implications for the distribution of fluids, *Geology*, *34*(1), 53–56.
Syracuse, E. M., P. E. van Keken, and G. A. Abers (2010), The global range of subduction zone thermal models, *Phys. Earth Planet. Inter.*, *183*(1–2), 73–90.
van Keken, P. E., B. R. Hacker, E. M. Syracuse, and G. A. Abers (2011), Subduction factory: 4. Depth-dependent flux of H_2O from subducting slabs worldwide, *J. Geophys. Res.*, *116*, B01401, doi:10.1029/2010JB007922.
Wang, D., and S. Karato (2013), Electrical conductivity of talc aggregates at 0.5 GPa: Influence of dehydration, *Phys. Chem. Miner.*, *40*, 11–17.
Wang, D., Y. Guo, Y. Yu, and S. Karato (2012), Electrical conductivity of amphibole-bearing rocks: Influence of dehydration, *Contrib. Mineral. Petrol.*, *164*, 17–25.
Wannamaker, P. E., T. G. Caldwell, G. R. Jiracek, V. Maris, G. J. Hill, Y. Ogawa, H. M. Bibby, S. L. Bennie, and W. Heise (2009), Fluid and deformation regime of an advancing subduction system at Marlborough, New Zealand, *Nature*, *460*(7256), 733–736.
Worzewski, T., M. Jegen, H. Kopp, H. Brasse, and W. T. Castillo (2011), Magnetotelluric image of the fluid cycle in the Costa Rican subduction zone, *Nat. Geosci.*, *4*(2), 108–111.
Yang, X., H. Keppler, C. McCammon, and H. Ni (2012), Electrical conductivity of orthopyroxene and plagioclase in the lower crust, *Contrib. Mineral. Petrol.*, *163*(1), 33–48.
Yoshino, T., A. Shimojuku, S. Shan, X. Guo, D. Yamazaki, E. Ito, Y. Higo, and K. Funakoshi (2012), Effect of temperature, pressure and iron content on the electrical conductivity of olivine and its high-pressure polymorphs, *J. Geophys. Res.*, *117*, B08205, doi:10.1029/2011JB008774.